Biogenic emissions and nocturnal ozone depletion events at the Amphitrite Point Observatory on Vancouver Island

T. W. Tokarek[1], D. K. Brownsey[1], N. Jordan[1], N. M. Garner[1], C. Z. Ye[1], F. V. Assad,[1] A. Peace[1], C. L. Schiller[2], R. H. Mason[2], R. Vingarzan[2], and H. D. Osthoff[1]*

[1] *Department of Chemistry, University of Calgary, Calgary, AB T2N 1N4, Canada*

[2] *Science Division, Environment and Climate Change Canada, Meteorological Services, Prediction and Services Operations West, Vancouver, British Columbia, Canada*

Corresponding author's email: hosthoff@ucalgary.ca

Biogenic emissions and nocturnal ozone depletion events at the Amphitrite Point Observatory on Vancouver Island

Routine monitoring stations on the west coast of North America serve to monitor baseline levels of criteria pollutants such as ozone (O_3) arriving from the Pacific Ocean. In Canada, the Amphitrite Point Observatory (APO) on Vancouver Island has been added to this network to provide regional baseline measurements. In 2014, McKendry and co-workers reported frequent nocturnal O_3 depletion events (ODEs) at APO that generally correlated with alongshore winds, elevated concentrations of carbon dioxide (CO_2) and stable boundary layer conditions, but whose cause (or causes) has (have) remained unclear.

This manuscript presents results from the Ozone-depleting Reactions in a Coastal Atmosphere (ORCA) campaign, which took place in July, 2015 to further investigate ODEs at APO. In addition to the long-term measurements at the site (e.g., of CO_2 and O_3 mixing ratios), abundances of biogenic volatile organic compounds (BVOC) and aerosol size distributions were quantified. ODEs were observed on the majority of measurement nights and were characterized by a simultaneous increase of CO_2 and BVOC abundances, in particular of limonene, a terpene 2.5× more reactive with respect to oxidation of O_3 than other monoterpenes.

Back trajectory calculations showed that ODEs occurred mainly in air masses that originated from the WNW where the air would have travelled parallel to the coastline and above kelp forests. Head space analyses of sea weed samples showed that bull kelp is a source of gas-phase limonene, consistent with its high relative abundance in air masses from the WNW sector. However, the enhanced terpene and CO_2 content showed that the air likely also came in contact with terrestrial vegetation via mesoscale transport phenomena (such as slope flows and land-sea breeze circulations) that were generally poorly captured by the back trajectories. This absence of aerosol growth during ODEs indicates that dry deposition is likely the primary O_3 loss mechanism.

Keywords: marine boundary layer, ozone depletion, coastal zone, monoterpene emissions, kelp, limonene

1. Introduction

Processes controlling the abundances of ozone (O_3) and fine particulate matter with a diameter smaller than 2.5 μm ($PM_{2.5}$) continue to be of interest because of the association of high O_3 and $PM_{2.5}$ concentrations with health impacts such as chronic obstructive pulmonary disease (COPD), heart disease, and lung cancer (e.g., (Lelieveld, Evans, Fnais, Giannadaki, & Pozzer, 2015; Peng et al., 2013; Pope, Ezzati, & Dockery, 2009) and references therein). On the west coast of North America, the budgets of O_3 and, indirectly, the hydroxyl radical (OH) and $PM_{2.5}$ depend critically on the "background O_3" concentration, i.e., the concentration of O_3 entering from the Pacific Ocean (Ambrose, Reidmiller, & Jaffe, 2011; McDonald-Buller et al., 2011). In recent decades, this concentration has slowly been increasing due to long-range transport of continuously rising emissions in Asia (Jaffe, Price, Parrish, Goldstein, & Harris, 2003; Parrish et al., 2010; Parrish et al., 2004). On the other hand, the concentration of O_3 in the layer immediately above the ocean surface, the so-called marine boundary layer (MBL), is frequently depleted relative to atmospheric layers aloft. The principal O_3 depletion mechanisms in the MBL are dry deposition to the sea surface (Gallagher, Beswick, & Coe, 2001; Gallagher, Beswick, McFiggans, Coe, & Choularton, 2001; Ganzeveld, Helmig, Fairall, Hare, & Pozzer, 2009) and photochemical pathways, such as the HO_x driven O_3 destruction in low NO_x environments and catalytic cycles involving reactive halogen species (Galbally, Bentley, & Meyer, 2000; Lee et al., 2009; Read et al., 2008; Singh et al., 1996; Watanabe, Nojiri, & Kariya, 2005).

The Amphitrite Point Observatory (APO) was established on the west coast of Vancouver Island, British Columbia, Canada, in 2010 to serve as a background monitoring site. Recently, McKendry and co-workers (2014) reported observations of rapid nocturnal O_3 depletion events (ODEs) that have not been fully explained to date. Conventionally, nocturnal loss of surface O_3 is interpreted as being due to a

70 combination of dry deposition and chemical titration by nitric oxide (NO) to nitrogen
71 dioxide (NO_2) and by reaction of O_3 with unsaturated biogenic hydrocarbons (Kleinman
72 et al., 1994; Logan, 1989; Neu, Kunzle, & Wanner, 1994; Trainer et al., 1987). At APO,
73 the ODEs are generally associated with along- or onshore flow, stable boundary layer
74 conditions, and an increase in the concentration of carbon dioxide (CO_2) but not with
75 anthropogenic pollution tracers, i.e., NO_x, CO, and SO_2 (McKendry et al., 2014). CO_2
76 has sinks (photosynthesis) and sources (respiration and combustion) that are much
77 stronger in the continental compared to the marine environment (which is a net CO_2
78 sink (Gruber et al., 2009)). Hence, elevated concentrations of CO_2 trace continentally
79 influenced air at coastal sites (Parrish, Millet, & Goldstein, 2009). The correlation of
80 ODEs with CO_2 and the absence of correlations with anthropogenic tracers at APO
81 suggest that the upwind air had been in contact with vegetation where O_3 would have
82 been more rapidly deposited than to the ocean surface (Gallagher, Beswick, & Coe,
83 2001; Wesely & Hicks, 2000). Yet, back trajectories calculated using the Hybrid Single
84 Particle Lagrangian Integrated Trajectory Model (HYSPLIT) (Draxler & Hess, 1998;
85 Draxler & Rolph, 2011) and the "North American Meso" (NAM) meteorological field at
86 12 km resolution were inconsistent with this interpretation. The back trajectories
87 showed that ODEs were characterized by light onshore or alongshore winds and that the
88 air masses generally originated in the MBL, i.e., had a marine origin. Overall, the
89 evidence indicated that the ODEs at APO are caused by a non-photochemical coastal
90 zone process that extends over a spatial scale of tens of kilometres (McKendry et al.,
91 2014).
92 One such process could be the natural nocturnal O_3 deposition on near-shore
93 forest vegetation coupled with a nocturnal land breeze that mixes continentally
94 influenced air against the predominant westerly synoptic flow. This process is in all

likelihood poorly captured by the meteorological fields and, hence, HYSPLIT trajectories. Evidence to corroborate this hypothesis would be an enhancement of biogenic volatile organic compound (BVOC) concentrations, in particular of monoterpenes whose emissions have both a light-dependent (photosynthetic) as well as a light-independent fraction which (unlike those of isoprene) continue at night (Fares et al., 2013; Guenther et al., 2012). The tree species in the region are predominantly coniferous and include Western Red Cedar (*Thuja plicate*), Coastal Douglas Fir (*Psudotsuga menziesii ssp. menziesii*) and Western Hemlock (*Tsuga mertensiana*) (Mason et al., 2015). Monoterpenes ($C_{10}H_{16}$), in particular α- and β-pinene, dominate BVOC emissions from this type of vegetation (Burney & Jacobs, 2012; Copeland, Cape, Nemitz, & Heal, 2014; Drewitt, Curren, Steyn, Gillespie, & Niki, 1998; Geron, Rasmussen, Arnts, & Guenther, 2000; Helmig, Daly, Milford, & Guenther, 2013; Lagalante & Montgomery, 2003; Sakulyanontvittaya, Duhl, et al., 2008).

In this work, mixing ratios of the monoterpenes α- and β-pinene, limonene, carene, and terpinolene, as well as the β-pinene oxidation product nopinone ($C_9H_{14}O$) were quantified at APO for the first time to provide further insight into the cause (or causes) of the nocturnal ODEs during summertime. Nopinone is produced from the reaction of O_3 with β-pinene in ~50% yield (Jenkin, 2004) and is thus a direct tracer of O_3-monoterpene chemical reactions, though it is also produced (and destroyed) during the daytime from reactions initiated by OH (Barthelmie & Pryor, 1999; Jaoui & Kamens, 2003; Kavouras, Mihalopoulos, & Stephanou, 1999; Larsen et al., 2001). The data set includes measurements of aerosol size distributions as an indirect probe of O_3-monoterpene chemistry which results in the production of non-volatile material and manifests itself by either new particle formation or growth (Ehn et al., 2014; Griffin, Cocker, Flagan, & Seinfeld, 1999; Sakulyanontvittaya, Guenther, Helmig, Milford, &

Wiedinmyer, 2008). Correlations of ODEs with CO_2 and BVOC concentrations are presented. Sources of BVOCs in the region and implications of the data for the interpretation of ODEs at APO are discussed.

2. Methods

a. Study overview

The APO is located on the west coast of Vancouver Island south of the town of Ucluelet at 48.92° N and 125.54° W (Figure 1) less than 100 m from the high tide line of the Pacific Ocean. It was the location of several recent measurement intensives, and the immediate vicinity of the measurement site has been described comprehensively in the associated manuscripts (Mason et al., 2015; McKendry et al., 2014; Wilson et al., 2015; Yakobi-Hancock et al., 2014). For this study, named the "Ozone-depleting Reactions in a Coastal Atmosphere" (ORCA) campaign, instrumentation was housed in two mobile laboratories separated by a distance of approximately 15 m: one was operated by Environment Canada, British Columbia's Ministry of the Environment, and Metro Vancouver, whose measurement suite (which include a Licor 820 CO_2 monitor) has been described elsewhere (Mason et al., 2015; McKendry et al., 2014; Wilson et al., 2015; Yakobi-Hancock et al., 2014). The other was operated by the University of Calgary, whose measurements are described below. Meteorological parameters were measured at the Amphitrite Lighthouse (located halfway between the main field site and the ocean) and by a weather station (Vaisala WXT520) operated at a height above ground of 5.2 m atop the University of Calgary mobile laboratory. Off-shore meteorological data were collected at a moored buoy (C46206, located at La Perouse Bank 35 km WSW of APO) as described by Mason et al. (2015). Data were collected from July 8 - 31, 2015.

b. Gas phase measurements

Mixing ratios of BVOCs and nopinone were quantified using a commercial gas chromatograph equipped with a cylindrical ion-trap mass analyzer (Patterson et al., 2002; Riter et al., 2002) and electron impact ionization (Griffin 450 GC-MS). This instrument sampled from a 6.5 m long and 0.635 cm outer diameter (o.d.) stainless steel inlet from a height of 4.3 m above ground. A 3 m long section of the inlet was heated to 125 °C to remove interference due to O_3 (Hellén, Kuronen, & Hakola, 2012; Pollmann, Ortega, & Helmig, 2005). Air samples were pre-concentrated for 8 minutes at a flow rate of 213 mL min^{-1} on a dual sorbent trap containing Tenax TA and Carboxen 1017 held at 40 °C and were desorbed at a temperature of 240 °C onto a 30 m (length) × 0.25 mm (inner diameter) × 0.25 μm (film thickness) DB-5MS column operated with helium carrier gas (Praxair, ECD grade) purified using a triple trap (Restek 22464). The GC oven was programmed as follows: hold at 40° C for 3.00 min, heat at 3° C min^{-1} to 70° C and hold for 2.00 min, and heat at 15° C min^{-1} to 200 °C and hold for 2.00 min (total 25.67 min). This was followed by a 5.00 min recovery time to allow the oven and preconcentration trap to cool back to 40 °C. Full mass spectra (*m/z* from 35 to 425 Da) were collected at a rate of ~ 3 Hz. Retention times and indices, quantification ions, and limits of detection of the monoterpenes monitored are summarized in Table S-1.

The instrument was calibrated using mass flow controllers and a gas cylinder filled with a standard VOC mixture prepared in-house on July 2, 2015, a week prior to the campaign. This working standard was prepared by quantitatively transferring a 50 VOC component calibration mixture (Supelco 49148-U) containing α-pinene, β-pinene and limonene in methanol to an evacuated aluminum cylinder (supplied by Scott-Marrin; internal volume 29.50±0.33 L) which was subsequently pressurized with nitrogen gas to a pressure of 8500±250 kPa. The accuracy of this standard was

compound dependent and calculated from the concentration uncertainties provided by Supelco and uncertainty of the dilution volume and was 9.6% on average (range 8.3% to 12.0%). The uncertainties in the amounts delivered from this cylinder are increased further due to uncertainties in the flow delivered by the mass flow controllers to a total of ~11% on average. This error analysis assumes quantitative delivery of the VOCs through the 2-stage cylinder pressure regulator and the all-metal mass flow controller (a reasonable assumption following a several day long break-in period). Not included in this uncertainty is the potential loss (or production) of terpenes within the cylinder over the course of this campaign, which are expected to be small in a one month old aluminum cylinder but can be substantial, especially over longer time periods (e.g., (Apel et al., 1999; Jones, Kato, Nakashima, & Kajii, 2014; Rhoderick, 2010; Rhoderick & Lin, 2013)).

Between July 16 and 31, 2015, five "full" calibrations, i.e., with ≥ 5 points on the calibration curve measured in random order (including a "blank"), were performed. For the monoterpenes, the slopes of the calibration curves had relative standard deviations in the range of ±3.2% to ±22.6% (average 8.0%) and intercepts whose value ± 1 standard error encompassed zero. The response factors were linearly interpolated between calibration points.

The precision of the GC-MS was determined from the standard deviation of repeated measurements of a small amount of β-pinene evaporated into a 4,000 L smog chamber to an approximate mixing ratio of ~100 pptv and was ±3.4%.

It has been reported that monoterpenes can undergo rearrangement reactions during the thermal desorption process following preconcentration on Tenax (Arnts, 2010). In post-campaign experiments, approximately 1.5% of trapped β-pinene was found to isomerize to limonene, α-pinene, and camphene during desorption on our

instrument. Because this process happens during both calibration and ambient measurement of β-pinene, its effect is included in the instrumental response factor. In contrast to β-pinene, no rearrangement products were observed for either limonene or α-pinene.

Assuming that the above uncertainties are independent from each other and neglecting the potential degradation of monoterpenes within the standard gas cylinder, the total uncertainty (at the 1σ level) of the monoterpene measurements presented is ±15%, driven by the systematic uncertainty in the preparation of (and delivering a calibrated gas flow from) the standard gas cylinder (±11%), the standard uncertainties in the slopes of the calibration curves (±8%), and the measurement precision (±3.4%).

Not included in this uncertainty estimate are potential systematic errors arising from the interpolation between calibration points.

The response factors for carene and nopinone were determined prior to and after the campaign relative to that of α-pinene; the uncertainty of their mixing ratios was estimated at ±30%.

Other gas-phase measurements in the University of Calgary mobile laboratory included a UV absorption O_3 analyzer (Thermo Scientific 49i), a total odd nitrogen (NO_y) chemiluminescence analyzer (Thermo Scientific 42i), and a multi-channel cavity ring-down spectrometer for quantification of NO_2 and NO_x constructed in-house (Odame-Ankrah, 2015; Paul & Osthoff, 2010).

c. Particle phase measurements

Submicron and supermicron size distributions were monitored using a scanning mobility particle sizer (SMPS, TSI 3936L75) operated with butanol and an aerodynamic particle sizer (APS, TSI 3321). The SMPS sampled through a 1 μm cut-off impactor (0.071 cm internal diameter) via 3/8" o.d. conductive silicon tubing secured next to the

GC-MS inlet. The APS was operated from the container located on top of the trailer and sampled from a 1.6 m tall ½ o.d. aluminum tube (4.4 m AGL) whose tip was bent into a U-shape to prevent precipitation from entering the inlet. Both instruments were calibrated by the manufacturer but not in the field (e.g., inlet transmission efficiencies were not characterized), such that the aerosol size distributions are semi-quantitative.

d. Photolysis frequencies

Photolysis frequencies were determined by solar actinic flux spectroradiometry (Hofzumahaus, Kraus, & Muller, 1999) using a commercial radiometer with 2π receptor optics and photo diode array (PDA) detector (Metcon; 512 pixels, wavelength range 285 nm - 690 nm) which had been calibrated by the manufacturer. The spectrometer was mounted facing up (zenith view) to measure the down-dwelling radiation. The spectrometer was inverted periodically to determine the up-dwelling radiation. Photolysis frequencies were calculated using reference spectra and quantum yields from the NASA-JPL evaluation (Sander et al., 2010) and updated $ClNO_2$ cross-sections (Ghosh, Papanastasiou, Talukdar, Roberts, & Burkholder, 2011).

e. Back trajectory calculations

Twelve-hour back trajectories were calculated using the National Oceanic and Atmospheric Administration (NOAA) HYSPLIT online model and the "NAM meteorological field at 12 km resolution. The trajectory calculations were initiated every hour, starting 1 hr prior to the ODEs and ending 1 hr after the ODEs ended, with heights of 10 m, 50 m, and 100 m above ground.

3. Results and analysis

a. Identification of ozone depletion events

Time series of O_3 and CO_2, the monoterpenes α- and β-pinene, limonene, and carene as well as the β-pinene oxidation product nopinone, NO_2 and odd oxygen (O_x = O_3 + NO_2) for the period of July 16 to 31, 2015 are shown in Figure 2. Time series of meteorological parameters are shown in Figure S-1. McKendry et al. (2014) outlined the following criteria to identify ODEs: a drop in O_3 mixing ratio from a starting value of no higher than 32 ppbv (the third monthly quartile O_3 mixing ratio in July), by more than 15 ppbv, and occurring over a time period of 12 hours or less. Using these criteria for the 16 nights shown, 9 nocturnal ODEs were identified. These are indicated as blue bars in Figure 2 and have been summarized in Table 1. The high frequency of ODEs confirms that they are indeed a frequent phenomenon at APO.

b. Correlations of ozone depletion events with chemical tracers

The ODEs were accompanied by an increase in CO_2 mixing ratios (Figures 2A and 5B), as had been reported by McKendry et al. (2014). At the beginning of the ODEs, CO_2 mixing ratios were usually below 380 ppmv. This abundance is less than what was measured at Trinidad Head, California in July, 2015 (396±1 ppmv). (Dlugokencky et al., 2016) Plausible explanations for the lower than expected CO_2 mixing ratios are either a prolonged period of CO_2 oceanic uptake in a decoupled marine boundary layer and/or photosynthetic uptake by vegetation upwind of the measurement location.

Once the ODEs started and O_3 mixing ratios decreased, CO_2 mixing ratios increased. Data from all nine ODEs were lumped together in one-hour bins as a function of time of day, with 12:00 (noon) set to the solar zenith angle minimum. The 90^{th}, 75^{th}, 25^{th}, and 10^{th} percentile and median (i.e., 50^{th} percentile) O_3 and CO_2 mixing ratios as

functions of local time of day during the ODEs are shown in Figure 3A. The median O_3 and CO_2 mixing ratios are anti-correlated with a linear correlation coefficient of r = -0.92 and slope of (-0.390±0.005) ppbv O_3 / ppmv CO_2.

It is well known that forest vegetation represents a sink of O_3 and, because of the absence of O_3 production, results in a net loss of O_3 at night (Trainer et al., 1987; Turner, Waggoner, & Rich, 1974). The observed anti-correlation can be rationalized by respiration by vegetation, which releases CO_2 into a shallow nocturnal boundary layer; at the same time, O_3 deposition continues, though with reduced deposition velocity (Fan, Wofsy, Bakwin, Jacob, & Fitzjarrald, 1990; Monson & Holland, 2001; Ro-Poulsen, Mikkelsen, Hovmand, Hummelsehoj, & Jensen, 1998; Zeller & Nikolov, 2000).

Since trees continue to emit monoterpenes at night, the nocturnal release of CO_2 from trees is expected to be accompanied by an increase in monoterpene concentration. Accordingly, mixing ratios of monoterpenes were also elevated during ODEs, coinciding with the increase in CO_2 (Figures 2B, 3B and 5B). The highest monoterpene mixing ratios were observed during the ODEs of the nights of July 18/19 and 19/20. Carene and nopinone mixing ratios were elevated on those nights (Figure 2B). The HYSPLIT back trajectories showed that the air masses sampled on those nights originated from the east (Table 1), i.e., had travelled over land covered by dense forests, explaining the higher than average monoterpene mixing ratios and also the presence of the β-pinene oxidation product nopinone.

The linear correlation coefficient of CO_2 and total monoterpene concentrations during ODEs was r = 0.93, whereas that of O_3 and total monoterpenes was r = -0.76. CO_2 is a more conserved tracer than monoterpenes which are oxidized by O_3 (and the nitrate radical, NO_3). The nopinone mixing ratios (Figure 2B) did not increase during

ODEs (Figure 4B), with exception of the nights of July 18/19 and 19/20, which indicates that titration of O_3 in the gas-phase was a minor O_3 depletion process and suggests that O_3 is lost more by dry deposition than by titration in the gas-phase. This conclusion is supported by the absence of new particle formation and aerosol growth during the ODEs (see section c below).

In polluted areas, O_3 mixing ratios are often depleted due to titration of O_3 by NO, which manifests itself by an anti-correlation of O_3 and NO_2 mixing ratios (Kleinman et al., 1994; Logan, 1989; Neu et al., 1994; Trainer et al., 1987). In contrast to CO_2 and monoterpenes, O_3 mixing ratios only correlated weakly with those of the anthropogenic pollution tracer NO_2 ($r = -0.44$). A scatter plot of O_3 against NO_2 mixing ratios is shown in Figure 5C, where the data points collected during ODEs are colour-coded by CO_2 mixing ratio. The vast majority of data points during ODEs are associated with NO_2 mixing ratios < 2 ppbv. Hence, the contribution of NO-O_3 titration to ozone depletion was minor.

This conclusion is corroborated by considering trends in O_x which parallel those of O_3 (Figure 2C). When O_x (instead of O_3) is correlated with total monoterpenes during ODEs, the anti-correlation becomes more pronounced ($r = -0.78$ compared to -0.76). In contrast, the anti-correlation of O_x with CO_2 changes to $r = -0.81$ (from -0.92), likely because NO_2 and CO_2 are both present in combustion exhaust where they correlate.

Overall, the correlations of O_3 with chemical tracers corroborate the notion that ODEs are not driven primarily by anthropogenic pollutants and that ODEs occur in air masses that have been in contact with respiring vegetation.

c. Role of meteorology

The ODEs were generally marked by a reduction in local wind speed (Figures S1 and 5A). The lowest O_3 mixing ratios were observed when the air stagnated (Figure

316 5A). This suggests that ODEs are caused by a local mechanism and are not
317 representative of a process occurring over a wider scale. There was no correlation of
318 ODEs with tide height (data not shown).
319 Synoptic conditions during the ODEs, judged from composite sea level pressure
320 and geopotential height and their anomaly maps obtained from the National Oceanic
321 and Atmospheric Administration's Physical Sciences Division's web site (Figure S-2)
322 were similar to those reported by McKendry et al. (2014), in that they show a high
323 pressure region centered north of the Hawaiian Islands in the Pacific Ocean, with a
324 developing high-pressure ridge aligned along the Pacific Northwest coast. Though not
325 as pronounced as shown by McKendry et al. (2014), this high pressure region extends
326 above the measurement site on Vancouver Island. The anticyclonic (i.e., clockwise
327 rotation) conditions (Figure S2) are expected to be associated with predominantly
328 WNW to NW winds in the study region as well as downward advection of warmer, dry
329 air from the upper troposphere in the anticyclone's center, leading to greater temperature
330 inversion and capping of the boundary layer throughout the high-pressure system (Stull
331 & Ahrens, 2000).
332 McKendry et al. (2014) had based much of their analysis on HYSPLIT back
333 trajectories with the NAM met field. Tables S-2 through S-10 summarize the hourly
334 HYSPLIT back trajectory data for this data set. By and large, the HYSPLIT results were
335 in agreement with local wind direction, with exception of July 27, when the flow
336 reversed (from on-shore to off-shore flow) in the middle of the night which was not
337 captured by the HYSPLIT trajectories. The ends of the ODEs were generally also
338 marked by a change (often a reversal) of local wind direction, which also were not
339 captured by HYSPLIT trajectories (e.g., on July 16, 23, 30). This suggests that the
340 meteorological field only poorly captures the land breeze (which goes against the

synoptic westerly flow), and that the HYSPLIT back trajectories do not capture injections of continentally influenced air into the coastal MBL.

Corroborating this are the relative humidity (RH) data. Often, the RH in HYSPLIT was inconsistent with local observations. For example, during the ODEs on July 18 and 19 and 30, local RH were >80%, whereas those in the simulations were <65%. A lower RH indicates an air mass that has travelled more over (dry) land than over the ocean. Interestingly, the nights of July 18, 19, and 30 had the highest CO_2 and total monoterpene abundances, which is consistent with the air having been in contact with land upwind. In general, RH decreased at the end of the ODEs as the air masses shifted.

The majority of the ODEs were associated with winds from the WNW, i.e., with air that has travelled in parallel to the coast line, consistent with the synoptic conditions. The nights of July 21 and 22 are interesting cases in that on both occasions, local winds and HYSPLIT back trajectories were from the WNW sector and wind speeds decreased (to < 1 m/s on July 22), yet O_3 was conserved on those nights. One can conclude that the HYSPLIT back trajectories by themselves are poor predictors of ODEs. The NOAA ESRL maps show that the high pressure region was located significantly further from the coast on those days ((Figure S-3) than during ODE events and that a low pressure system had formed to the North of the study region.

c. Correlations of ODEs with changes in aerosol size distribution

Reactions of O_3 with monoterpenes are known to yield SOA (Ehn et al., 2014; Griffin et al., 1999; Sakulyanontvittaya, Guenther, et al., 2008). The time series of submicron aerosol size distributions is shown in Figure 6. During the ODEs, the accumulation mode (diameter range 80 to 100 nm) dominated. The highest counts were observed when the predominant wind direction was from the east (nights of July 18/19

and 19/20), whereas much lower aerosol loadings were observed when the winds were from the West. With exception of the night of July 19/20, there was neither noticeable particle growth nor nucleation event during the ODEs. The absence of aerosol growth and new particle formation corroborates that dry deposition is the primary O_3 loss mechanism and that titration of O_3 by gas-phase monoterpenes (which would have yielded SOA and nopinone) was minor. However, new particles were frequently observed after the ODEs ended, usually associated with a wind shift to the east at or after sunrise.

e. Monoterpene ratios: insights into BVOC sources

An interesting feature of this data set is that the limonene mixing ratio was often greater than those of α- and β-pinene (and sometimes even greater than their sum). Limonene is a factor of 2.5× more reactive than the other monoterpenes with respect to oxidation by O_3 and NO_3 (Draper, Farmer, Desyaterik, & Fry, 2015). The high relative concentrations of limonene observed suggest that the air had not been significantly processed ("aged") chemically, which implies that the source (or sources) of limonene was (were) close to the sampling site. Carene and terpinolene were less abundant than the other monoterpenes and accounted for only a small fraction of the total concentration of terpenes observed (Figure 4A). Only one of the common tree species in the area, the Western Red Cedar, emits a greater amount of limonene than other monoterpenes (Drewitt et al., 1998); its emission ratios are most consistent with the observed monoterpene mixtures. In contrast, emissions from Coastal Douglas Firs are expected to have a higher α- and β-pinene content and relatively little limonene (Burney & Jacobs, 2012; Geron et al., 2000), and emissions from Western Hemlock trees have a high α - and β-pinene as well as phellandrene content (Lagalante & Montgomery, 2003), which are less consistent with the relative terpene concentrations observed.

Oddly, there was a dependence of the monoterpene ratios on local wind direction during the ODEs; when local wind speeds were strongest and from the WNW, the ratios of limonene to α- and β-pinene were highest (Figure 5D). The ocean surface is a known (though small) source of a variety of volatile compounds (Carpenter, Archer, & Beale, 2012), including unsaturated compounds such as isoprene (Meskhidze & Nenes, 2006; Yokouchi, Li, Machida, Aoki, & Akimoto, 1999) and monoterpenes (Yassaa et al., 2008). However, one local peculiarity at APO is the presence of kelp forests along the coast line (Watson & Estes, 2011).

f. Kelp forests: an unrecognized source of BVOCs

There is currently very little literature on BVOC emissions from near-shore vegetation. *Yassaa and coworkers* recently reported evidence for monoterpene emissions from phytoplankton (*Dunaliella tertiolecta*), in which p-ocimene, limonene, and camphene were the dominant monoterpenes emitted (Yassaa et al., 2008). Kelp is known to emit molecular iodine and small molecule halocarbons (e.g., (Ball et al., 2010; Dixneuf, Ruth, Vaughan, Varma, & Orphal, 2009; Nitschke, Dixneuf, Schmid, Ruth, & Stengel, 2015; Weinberg, Bahlmann, Michaelis, & Seifert, 2013)). These iodine emissions and their subsequent chemistry have been linked to near-coastal new particle formation (O'Dowd et al., 2002; O'Dowd & Hoffmann, 2005) though uncertainties remain (e.g., (McFiggans, 2005; O'Dowd et al., 2005).

To investigate whether local sea weed species contributed to BVOC emissions, samples were collected from the intertidal zone, placed in buckets along with sea water, and the head spaces were analyzed by GC-MS.

Total and selected ion chromatograms of the calibration VOC mixture, of ambient air during ODEs with a strong westerly flow, and of the head space above a sample of bull kelp (*Nereocystis luetkeana*) are shown in Figure 7. The selected ion *m/z*

93(±1) is a characteristic fragment of monoterpenes ($C_7H_9^+$). The bull kelp head space (Figure 7C) contained ~2 ppbv limonene and trace amounts of α- and β-pinene and terpinolene. Terpenes were not elevated when a sample of sea water in the absence of sea flora was analyzed (data not shown). This implies that the kelp forests act as a source of limonene and (at least partially) explains the high relative limonene abundances observed during ODEs where the air originated from WNW sector.

We currently do not have enough information to constrain this source (e.g., size of the kelp forests and their emission rates, which depend on time-of-day, water temperature, light and herbivore exposure, plant age, season, and the extent of desiccation and degradation of kelp deposited near the high tide mark (Bravo-Linares, Mudge, & Loyola-Sepulveda, 2010; Nitschke et al., 2015; Rodgers & Shears, 2016)), though it clearly would be worthwhile to investigate these factors further. Of all the biogenic terpenes, limonene exhibits the highest SOA yield upon photo-oxidation (Griffin et al., 1999; Hoffmann et al., 1997) and upon reaction with O_3 or NO_3 at night (Draper et al., 2015; Fry et al., 2011; Spittler et al., 2006). It stands to reason that emissions of limonene coupled to those of molecular iodine from the same source would have high SOA formation potential.

4. Summary and conclusions

This study has shown that the ODEs observed at APO occurred in air masses that had been in contact with near-coastal vegetation including kelp forests and trees located near the shore line. Even though this data set was limited to one month during summer, it can be expected that the O_3-terpene anticorrelation will also be observed during other seasons as terpene emissions continue throughout the year and peak in spring (Helmig et al., 2013). The absence of aerosol growth and new particle formation associated with

ODEs indicates that dry deposition was likely the primary O_3 loss mechanism and that titration of O_3 by gas-phase monoterpenes was a minor pathway. At the same time, more measurements, in particular of terpenoids towards which O_3 is reactive such as the sesquiterpenes (Sakulyanontvittaya, Duhl, et al., 2008), are needed to better constrain their roles in O_3 depletion, especially within the forest canopy. However, the absence of organic aerosol formation during ODEs suggests that reactions of O_3 with biogenic VOCs were of minor importance during this campaign. Back trajectories calculated using HYSPLIT and the NAM meteorology field poorly represented local coastal land-sea breeze effects and hence fell short in explaining how the upwind air at APO came in contact with continentally influenced air masses.

Future studies should focus on a better description of the regional flow patterns and should aim to quantify the relative contributions of terrestrial and oceanic surfaces to O_3 dry deposition, the potential for halogen-catalyzed photochemical destruction of O_3 (e.g., (Huang et al., 2010)), and the exchange of CO_2 with surfaces and vegetation in the region. Future studies should also elucidate whether near-costal oceanic uptake of O_3 is enhanced in the region, for example by elevated iodide surface concentrations (Carpenter et al., 2013; Reeser & Donaldson, 2011). Kelp forests were identified as a novel BVOC source that emits highly reactive terpenes such as limonene. Future work should focus on characterizing the emission factors of BVOCs from kelp and other sea weed species.

461 References

462

463 Ambrose, J. L., Reidmiller, D. R., & Jaffe, D. A. (2011). Causes of high O_3 in the lower free
464 troposphere over the Pacific Northwest as observed at the Mt. Bachelor Observatory.
465 *Atmospheric Environment, 45*(30), 5302-5315. doi: 10.1016/j.atmosenv.2011.06.056

466 Apel, E. C., Calvert, J. G., Gilpin, T. M., Fehsenfeld, F. C., Parrish, D. D., & Lonneman, W. A.
467 (1999). The Nonmethane Hydrocarbon Intercomparison Experiment (NOMHICE): Task
468 3. *Journal of Geophysical Research, 104*(D21), 26,069–026,086. doi:
469 10.1029/1999jd900793

470 Arnts, R. R. (2010). Evaluation of adsorbent sampling tube materials and Tenax-TA for analysis
471 of volatile biogenic organic compounds. *Atmospheric Environment, 44*(12), 1579-1584.
472 doi: 10.1016/j.atmosenv.2010.01.004

473 Ball, S. M., Hollingsworth, A. M., Humbles, J., Leblanc, C., Potin, P., & McFiggans, G. (2010).
474 Spectroscopic studies of molecular iodine emitted into the gas phase by seaweed.
475 *Atmospheric Chemistry and Physics, 10*(13), 6237-6254. doi: 10.5194/acp-10-6237-
476 2010

477 Barthelmie, R. J., & Pryor, S. C. (1999). A model mechanism to describe oxidation of
478 monoterpenes leading to secondary organic aerosol - 1. alpha-pinene and beta-pinene.
479 *Journal of Geophysical Research, 104*(D19), 23657-23669. doi:
480 10.1029/1999JD900382

481 Bravo-Linares, C. M., Mudge, S. M., & Loyola-Sepulveda, R. H. (2010). Production of volatile
482 organic compounds (VOCs) by temperature macroalgae. The use of solid phase
483 microextraction (SPME) coupled to GC-MS as method of analysis. *Journal of the*
484 *Chilean Chemical Society, 55*(2), 227-232. doi: 10.4067/S0717-97072010000200018

485 Burney, O. T., & Jacobs, D. F. (2012). Terpene production and growth of three Pacific
486 Northwest conifers in response to simulated browse and nutrient availability. *Trees,*
487 *26*(4), 1331-1342. doi: 10.1007/s00468-012-0709-4

488 Carpenter, L. J., Archer, S. D., & Beale, R. l. (2012). Ocean-atmosphere trace gas exchange.
489 *Chemical Society Reviews, 41*(19), 6473-6506. doi: 10.1039/c2cs35121h

490 Carpenter, L. J., MacDonald, S. M., Shaw, M. D., Kumar, R., Saunders, R. W., Parthipan, R., . .
491 . Plane, J. M. C. (2013). Atmospheric iodine levels influenced by sea surface emissions
492 of inorganic iodine. *Nature Geoscience, 6*(2), 108-111. doi: 10.1038/ngeo1687

493 Copeland, N., Cape, J. N., Nemitz, E., & Heal, M. R. (2014). Volatile organic compound
494 speciation above and within a Douglas fir forest. *Atmospheric Environment, 94*(0), 86-
495 95. doi: 10.1016/j.atmosenv.2014.04.035

496 Dixneuf, S., Ruth, A. A., Vaughan, S., Varma, R. M., & Orphal, J. (2009). The time dependence
497 of molecular iodine emission from Laminaria digitata. *Atmospheric Chemistry and*
498 *Physics, 9*(3), 823-829. doi: 10.5194/acp-9-823-2009

499 Dlugokencky, E. J., Lang, P. M., Mund, J. W., Crotwell, A. M., Crotwell, M. J., & Thoning, K.
500 W. (2016). *Atmospheric Carbon Dioxide Dry Air Mole Fractions from the NOAA ESRL*
501 *Carbon Cycle Cooperative Global Air Sampling Network, 1968-2015, Version: 2016-*
502 *08-30*. Retrieved from ftp://aftp.cmdl.noaa.gov/data/trace_gases/co2/flask/surface/

503 Draper, D. C., Farmer, D. K., Desyaterik, Y., & Fry, J. L. (2015). A qualitative comparison of
504 secondary organic aerosol yields and composition from ozonolysis of monoterpenes at
505 varying concentrations of NO_2. *Atmospheric Chemistry and Physics, 15*(21), 12267-
506 12281. doi: 10.5194/acp-15-12267-2015

507 Draxler, R. R., & Hess, G. D. (1998). An overview of the HYSPLIT_4 modelling system for
508 trajectories, dispersion and deposition. *Australian Meteorological Magazine, 47*(4),
509 295-308

510 Draxler, R. R., & Rolph, G. D. (2011). *HYSPLIT (HYbrid Single-Particle Lagrangian*
511 *Integrated Trajectory) Model access via NOAA ARL READY Website* Retrieved from
512 http://ready.arl.noaa.gov/HYSPLIT.php

513 Drewitt, G. B., Curren, K., Steyn, D. G., Gillespie, T. J., & Niki, H. (1998). Measurement of
514 biogenic hydrocarbon emissions from vegetation in the Lower Fraser Valley, British
515 Columbia. *Atmospheric Environment, 32*(20), 3457-3466. doi: 10.1016/S1352-
516 2310(98)00043-0

517 Ehn, M., Thornton, J. A., Kleist, E., Sipila, M., Junninen, H., Pullinen, I., . . . Mentel, T. F.
518 (2014). A large source of low-volatility secondary organic aerosol. *Nature, 506*(7489),
519 476-479. doi: 10.1038/nature13032

520 Fan, S.-M., Wofsy, S. C., Bakwin, P. S., Jacob, D. J., & Fitzjarrald, D. R. (1990). Atmosphere-
521 biosphere exchange of CO_2 and O_3 in the central Amazon Forest. *Journal of*
522 *Geophysical Research: Atmospheres, 95*(D10), 16851-16864. doi:
523 10.1029/JD095iD10p16851

524 Fares, S., Schnitzhofer, R., Jiang, X., Guenther, A., Hansel, A., & Loreto, F. (2013).
525 Observations of Diurnal to Weekly Variations of Monoterpene-Dominated Fluxes of
526 Volatile Organic Compounds from Mediterranean Forests: Implications for Regional
527 Modeling. *Environmental Science & Technology, 47*(19), 11073-11082. doi:
528 10.1021/es4022156

529 Fry, J. L., Kiendler-Scharr, A., Rollins, A. W., Brauers, T., Brown, S. S., Dorn, H. P., . . .
530 Cohen, R. C. (2011). SOA from limonene: role of NO_3 in its generation and
531 degradation. *Atmospheric Chemistry and Physics, 11*(8), 3879-3894. doi: 10.5194/acp-
532 11-3879-2011

533 Galbally, I. E., Bentley, S. T., & Meyer, C. P. (2000). Mid-latitude marine boundary-layer
534 ozone destruction at visible sunrise observed at Cape Grim, Tasmania, 41°S.
535 *Geophysical Research Letters, 27*(23), 3841-3844. doi: 10.1029/1999gl010943

536 Gallagher, M. W., Beswick, K. M., & Coe, H. (2001). Ozone deposition to coastal waters.
537 *Quarterly Journal Of The Royal Meteorological Society, 127*(572), 539-558. doi:
538 10.1002/qj.49712757215

539 Gallagher, M. W., Beswick, K. M., McFiggans, G., Coe, H., & Choularton, T. W. (2001).
540 Ozone Dry Deposition Velocities for Coastal Waters. *Water, Air and Soil Pollution:*
541 *Focus, 1*(5), 233-242. doi: 10.1023/a:1013119524952

542 Ganzeveld, L., Helmig, D., Fairall, C. W., Hare, J., & Pozzer, A. (2009). Atmosphere-ocean
543 ozone exchange: A global modeling study of biogeochemical, atmospheric, and
544 waterside turbulence dependencies. *Global Biogeochemical Cycles, 23*(4), GB4021.
545 doi: 10.1029/2008gb003301

546 Geron, C., Rasmussen, R., Arnts, R. R., & Guenther, A. (2000). A review and synthesis of
547 monoterpene speciation from forests in the United States. *Atmospheric Environment*,
548 *34*(11), 1761-1781. doi: 10.1016/S1352-2310(99)00364-7

549 Ghosh, B., Papanastasiou, D. K., Talukdar, R. K., Roberts, J. M., & Burkholder, J. B. (2011).
550 Nitryl Chloride ($ClNO_2$): UV/Vis Absorption Spectrum between 210 and 296 K and
551 O(^{3}P) Quantum Yield at 193 and 248 nm. *Journal of Physical Chemistry A*, *116*(24),
552 5796-5805. doi: 10.1021/jp207389y

553 Griffin, R. J., Cocker, D. R., Flagan, R. C., & Seinfeld, J. H. (1999). Organic aerosol formation
554 from the oxidation of biogenic hydrocarbons. *Journal of Geophysical Research*,
555 *104*(D3), 3555-3567. doi: 10.1029/1998jd100049

556 Gruber, N., Gloor, M., Mikaloff Fletcher, S. E., Doney, S. C., Dutkiewicz, S., Follows, M. J., . .
557 . Takahashi, T. (2009). Oceanic sources, sinks, and transport of atmospheric CO_2.
558 *Global Biogeochemical Cycles*, *23*(1), GB1005. doi: 10.1029/2008gb003349

559 Guenther, A. B., Jiang, X., Heald, C. L., Sakulyanontvittaya, T., Duhl, T., Emmons, L. K., &
560 Wang, X. (2012). The Model of Emissions of Gases and Aerosols from Nature version
561 2.1 (MEGAN2.1): an extended and updated framework for modeling biogenic
562 emissions. *Geosci. Model Dev.*, *5*(6), 1471-1492. doi: 10.5194/gmd-5-1471-2012

563 Hellén, H., Kuronen, P., & Hakola, H. (2012). Heated stainless steel tube for ozone removal in
564 the ambient air measurements of mono- and sesquiterpenes. *Atmospheric Environment*,
565 *57*(0), 35-40. doi: 10.1016/j.atmosenv.2012.04.019

566 Helmig, D., Daly, R. W., Milford, J., & Guenther, A. (2013). Seasonal trends of biogenic
567 terpene emissions. *Chemosphere*, *93*(1), 35-46. doi:
568 10.1016/j.chemosphere.2013.04.058

569 Hoffmann, T., Odum, J. R., Bowman, F., Collins, D., Klockow, D., Flagan, R. C., & Seinfeld, J.
570 H. (1997). Formation of Organic Aerosols from the Oxidation of Biogenic
571 Hydrocarbons. *Journal of Atmospheric Chemistry*, *26*(2), 189-222. doi:
572 10.1023/a:1005734301837

573 Hofzumahaus, A., Kraus, A., & Muller, M. (1999). Solar actinic flux spectroradiometry: a
574 technique for measuring photolysis frequencies in the atmosphere. *Applied Optics*,
575 *38*(21), 4443-4460. doi: 10.1364/AO.38.004443

576 Huang, R. J., Seitz, K., Buxmann, J., Pohler, D., Hornsby, K. E., Carpenter, L. J., . . . Hoffmann,
577 T. (2010). In situ measurements of molecular iodine in the marine boundary layer: the
578 link to macroalgae and the implications for O_3, IO, OIO and NOx. *Atmospheric*
579 *Chemistry and Physics*, *10*(10), 4823-4833. doi: 10.5194/acp-10-4823-2010

580 Jaffe, D., Price, H., Parrish, D., Goldstein, A., & Harris, J. (2003). Increasing background ozone
581 during spring on the west coast of North America. *Geophysical Research Letters*,
582 *30*(12), 1613. doi: 10.1029/2003gl017024

583 Jaoui, M., & Kamens, R. M. (2003). Gaseous and particulate oxidation products analysis of a
584 mixture of alpha-pinene plus beta-pinene/O_3/air in the absence of light and alpha-pinene
585 plus beta-pinene/NO_x/air in the presence of natural sunlight. *Journal Of Atmospheric*
586 *Chemistry*, *44*(3), 259-297. doi: 10.1023/A:1022977427523

587 Jenkin, M. E. (2004). Modelling the formation and composition of secondary organic aerosol
588 from alpha- and beta-pinene ozonolysis using MCM v3. *Atmospheric Chemistry and*
589 *Physics, 4*, 1741-1757. doi: 10.5194/acp-4-1741-2004

590 Jones, C. E., Kato, S., Nakashima, Y., & Kajii, Y. (2014). A novel fast gas chromatography
591 method for higher time resolution measurements of speciated monoterpenes in air.
592 *Atmos. Meas. Tech., 7*(5), 1259-1275. doi: 10.5194/amt-7-1259-2014

593 Kavouras, I. G., Mihalopoulos, N., & Stephanou, E. G. (1999). Formation and gas/particle
594 partitioning of monoterpenes photo-oxidation products over forests. *Geophysical*
595 *Research Letters, 26*(1), 55-58. doi: 10.1029/1998GL900251

596 Kleinman, L., Lee, Y.-N., Springston, S. R., Nunnermacker, L., Zhou, X., Brown, R., . . .
597 Newman, L. (1994). Ozone formation at a rural site in the southeastern United States.
598 *Journal of Geophysical Research: Atmospheres, 99*(D2), 3469-3482. doi:
599 10.1029/93jd02991

600 Lagalante, A. F., & Montgomery, M. E. (2003). Analysis of Terpenoids from Hemlock (Tsuga)
601 Species by Solid-Phase Microextraction/Gas Chromatography/Ion-Trap Mass
602 Spectrometry. *Journal of Agricultural and Food Chemistry, 51*(8), 2115-2120. doi:
603 10.1021/jf021028s

604 Larsen, B. R., Di Bella, D., Glasius, M., Winterhalter, R., Jensen, N. R., & Hjorth, J. (2001).
605 Gas-phase OH oxidation of monoterpenes: Gaseous and particulate products. *Journal of*
606 *Atmospheric Chemistry, 38*(3), 231-276. doi: 10.1023/A:1006487530903

607 Lee, J. D., Moller, S. J., Read, K. A., Lewis, A. C., Mendes, L., & Carpenter, L. J. (2009). Year-
608 round measurements of nitrogen oxides and ozone in the tropical North Atlantic marine
609 boundary layer. *Journal of Geophysical Research, 114*, D21302. doi:
610 10.1029/2009jd011878

611 Lelieveld, J., Evans, J. S., Fnais, M., Giannadaki, D., & Pozzer, A. (2015). The contribution of
612 outdoor air pollution sources to premature mortality on a global scale. *Nature,*
613 *525*(7569), 367-371. doi: 10.1038/nature15371

614 Logan, J. A. (1989). Ozone in rural areas of the United States. *Journal of Geophysical*
615 *Research: Atmospheres, 94*(D6), 8511-8532. doi: 10.1029/JD094iD06p08511

616 Mason, R. H., Si, M., Li, J., Chou, C., Dickie, R., Toom-Sauntry, D., . . . Bertram, A. K. (2015).
617 Ice nucleating particles at a coastal marine boundary layer site: correlations with aerosol
618 type and meteorological conditions. *Atmospheric Chemistry and Physics, 15*(21),
619 12547-12566. doi: 10.5194/acp-15-12547-2015

620 McDonald-Buller, E. C., Allen, D. T., Brown, N., Jacob, D. J., Jaffe, D., Kolb, C. E., . . . Zhang,
621 L. (2011). Establishing Policy Relevant Background (PRB) Ozone Concentrations in
622 the United States. *Environmental Science & Technology, 45*(22), 9484-9497. doi:
623 10.1021/es2022818

624 McFiggans, G. (2005). Atmospheric science: Marine aerosols and iodine emissions. *Nature,*
625 *433*(7026), E13. doi: 10.1038/nature03372

626 McKendry, I. G., Christensen, E., Schiller, C., Vingarzan, R., Macdonald, A. M., & Li, Y.
627 (2014). Low Ozone Episodes at Amphitrite Point Marine Boundary Layer Observatory,
628 British Columbia, Canada. *Atmosphere-Ocean, 52*(3), 271-280. doi:
629 10.1080/07055900.2014.910164

630 Meskhidze, N., & Nenes, A. (2006). Phytoplankton and cloudiness in the Southern Ocean.
631 *Science, 314*(5804), 1419-1423. doi: 10.1126/science.1131779

632 Monson, R. K., & Holland, E. A. (2001). Biospheric Trace Gas Fluxes and Their Control Over
633 Tropospheric Chemistry. *Annual Review of Ecology and Systematics, 32*(1), 547-576.
634 doi: 10.1146/annurev.ecolsys.32.081501.114136

635 Neu, U., Kunzle, T., & Wanner, H. (1994). On the relation between ozone storage in the
636 residual layer and daily variation in near-surface ozone concentration — A case study.
637 *Boundary-Layer Meteorology, 69*(3), 221-247. doi: 10.1007/bf00708857

638 Nitschke, U., Dixneuf, S., Schmid, M., Ruth, A. A., & Stengel, D. B. (2015). Contribution of
639 living and degrading kelp to coastal iodine fluxes. *Marine Biology, 162*(9), 1727-1738.
640 doi: 10.1007/s00227-015-2699-4

641 O'Dowd, C. D., Jimenez, J. L., Bahreini, R., Flagan, R. C., Seinfeld, J. H., Hameri, K., . . .
642 Hoffmann, T. (2002). Marine aerosol formation from biogenic iodine emissions.
643 *Nature, 417*(6889), 632-636. doi: 10.1038/nature00775

644 O'Dowd, C. D., Jimenez, J. L., Bahreini, R., Flagan, R. C., Seinfeld, J. H., Hameri, K., . . .
645 Hoffmann, T. (2005). Marine aerosols and iodine emissions - Reply. *Nature, 433*(7026),
646 E13-E14. doi: 10.1038/nature03373

647 O'Dowd, C. D., & Hoffmann, T. (2005). Coastal New Particle Formation: A Review of the
648 Current State-Of-The-Art. *Environmental Chemistry, 2*(4), 245-255. doi:
649 10.1071/EN05077

650 Odame-Ankrah, C. A. (2015). *Improved detection instrument for nitrogen oxide species.*
651 (Ph.D.), University of Calgary, http://hdl.handle.net/11023/2006, Calgary.

652 Parrish, D. D., Aikin, K. C., Oltmans, S. J., Johnson, B. J., Ives, M., & Sweeny, C. (2010).
653 Impact of transported background ozone inflow on summertime air quality in a
654 California ozone exceedance area. *Atmospheric Chemistry and Physics, 10*(20), 10093-
655 10109. doi: 10.5194/acp-10-10093-2010

656 Parrish, D. D., Dunlea, E. J., Atlas, E. L., Schauffler, S., Donnelly, S., Stroud, V., . . . Roberts, J.
657 M. (2004). Changes in the photochemical environment of the temperate North Pacific
658 troposphere in response to increased Asian emissions. *Journal of Geophysical*
659 *Research, 109*(D23), D23S18. doi: 10.1029/2004jd004978

660 Parrish, D. D., Millet, D. B., & Goldstein, A. H. (2009). Increasing ozone in marine boundary
661 layer inflow at the west coasts of North America and Europe. *Atmospheric Chemistry*
662 *and Physics, 9*(4), 1303-1323. doi: 10.5194/acp-9-1303-2009

663 Patterson, G. E., Guymon, A. J., Riter, L. S., Everly, M., Griep-Raming, J., Laughlin, B. C., . . .
664 Cooks, R. G. (2002). Miniature Cylindrical Ion Trap Mass Spectrometer. *Analytical*
665 *Chemistry, 74*(24), 6145-6153. doi: 10.1021/ac020494d

666 Paul, D., & Osthoff, H. D. (2010). Absolute Measurements of Total Peroxy Nitrate Mixing
667 Ratios by Thermal Dissociation Blue Diode Laser Cavity Ring-Down Spectroscopy.
668 *Analytical Chemistry, 82*(15), 6695-6703. doi: 10.1021/ac101441z

669 Peng, R. D., Samoli, E., Pham, L., Dominici, F., Touloumi, G., Ramsay, T., . . . Samet, J.
670 (2013). Acute effects of ambient ozone on mortality in Europe and North America:
671 results from the APHENA study. *Air Quality, Atmosphere & Health, 6*(2), 445-453. doi:
672 10.1007/s11869-012-0180-9

673 Pollmann, J., Ortega, J., & Helmig, D. (2005). Analysis of Atmospheric Sesquiterpenes:
674 Sampling Losses and Mitigation of Ozone Interferences. *Environmental Science &*
675 *Technology, 39*(24), 9620-9629. doi: 10.1021/es050440w

676 Pope, C. A., Ezzati, M., & Dockery, D. W. (2009). Fine-Particulate Air Pollution and Life
677 Expectancy in the United States. *N Engl J Med, 360*(4), 376-386. doi:
678 10.1056/NEJMsa0805646

679 Read, K. A., Mahajan, A. S., Carpenter, L. J., Evans, M. J., Faria, B. V. E., Heard, D. E., . . .
680 Plane, J. M. C. (2008). Extensive halogen-mediated ozone destruction over the tropical
681 Atlantic Ocean. *Nature, 453*(7199), 1232-1235. doi: 10.1038/nature07035

682 Reeser, D. I., & Donaldson, D. J. (2011). Influence of water surface properties on the
683 heterogeneous reaction between O3(g) and I(aq)−. *Atmospheric Environment, 45*(34),
684 6116-6120. doi: http://dx.doi.org/10.1016/j.atmosenv.2011.08.042

685 Rhoderick, G. C. (2010). Stability assessment of gas mixtures containing terpenes at nominal
686 5 nmol/mol contained in treated aluminum gas cylinders. *Analytical and Bioanalytical*
687 *Chemistry, 398*(3), 1417-1425. doi: 10.1007/s00216-010-4058-0

688 Rhoderick, G. C., & Lin, J. (2013). Stability Assessment of Gas Mixtures Containing
689 Monoterpenes in Varying Cylinder Materials and Treatments. *Analytical Chemistry,*
690 *85*(9), 4675-4685. doi: 10.1021/ac400324v

691 Riter, L. S., Peng, Y. A., Noll, R. J., Patterson, G. E., Aggerholm, T., & Cooks, R. G. (2002).
692 Analytical performance of a miniature cylindrical ion trap mass spectrometer.
693 *Analytical Chemistry, 74*(24), 6154-6162. doi: 10.1021/ac0204956

694 Ro-Poulsen, H., Mikkelsen, T. N., Hovmand, M. F., Hummelsehoj, P., & Jensen, N. O. (1998).
695 Ozone deposition in relation to canopy physiology in a mixed conifer forest in
696 Denmark. *Chemosphere, 36*(4-5), 669-674. doi: 10.1016/s0045-6535(97)10105-9

697 Rodgers, K. L., & Shears, N. T. (2016). Modelling kelp forest primary production using in situ
698 photosynthesis, biomass and light measurements. *Marine Ecology Progress Series, 553*,
699 67-79. doi: 10.3354/meps11801

700 Sakulyanontvittaya, T., Duhl, T., Wiedinmyer, C., Helmig, D., Matsunaga, S., Potosnak, M., . . .
701 Guenther, A. (2008). Monoterpene and Sesquiterpene Emission Estimates for the
702 United States. *Environmental Science & Technology, 42*(5), 1623-1629. doi:
703 10.1021/es702274e

704 Sakulyanontvittaya, T., Guenther, A., Helmig, D., Milford, J., & Wiedinmyer, C. (2008).
705 Secondary Organic Aerosol from Sesquiterpene and Monoterpene Emissions in the
706 United States. *Environmental Science & Technology, 42*(23), 8784-8790. doi:
707 10.1021/es800817r

708 Sander, S. P., Abbatt, J. P. D., Barker, J. R., Burkholder, J. B., Friedl, R. R., Golden, D. M., . . .
709 Wine, P. H. (2010). *Chemical Kinetics and Photochemical Data for Use in Atmospheric*
710 *Studies, Evaluation No. 17*. Pasadena, CA: Jet Propulsion Laboratory.

711 Singh, H. B., Gregory, G. L., Anderson, B., Browell, E., Sachse, G. W., Davis, D. D., . . .
712 Merrill, J. (1996). Low ozone in the marine boundary layer of the tropical Pacific
713 Ocean: Photochemical loss, chlorine atoms, and entrainment. *Journal of Geophysical*
714 *Research, 101*(D1), 1907-1917. doi: 10.1029/95jd01028

715 Spittler, M., Barnes, I., Bejan, I., Brockmann, K. J., Benter, T., & Wirtz, K. (2006). Reactions of
716 NO_3 radicals with limonene and alpha-pinene: Product and SOA formation.
717 *Atmospheric Environment, 40*, S116-S127. doi: 10.1016/j.atmosenv.2005.09.093

718 Stull, R. B., & Ahrens, C. D. (2000). *Meteorology for scientists and engineers* (2nd ed.). Pacific
719 Grove, CA: Brooks/Cole.

720 Trainer, M., Williams, E. J., Parrish, D. D., Buhr, M. P., Allwine, E. J., Westberg, H. H., . . .
721 Liu, S. C. (1987). Models and observations of the impact of natural hydrocarbons on
722 rural ozone. *Nature, 329*(6141), 705-707. doi: 10.1038/329705a0

723 Turner, N. C., Waggoner, P. E., & Rich, S. (1974). Removal of ozone from the atmosphere by
724 soil and vegetation. *Nature, 250*(5466), 486-489. doi: 10.1038/250486a0

725 Watanabe, K., Nojiri, Y., & Kariya, S. (2005). Measurements of ozone concentrations on a
726 commercial vessel in the marine boundary layer over the northern North Pacific Ocean.
727 *Journal of Geophysical Research, 110*(D11), D11310. doi: 10.1029/2004jd005514

728 Watson, J., & Estes, J. A. (2011). Stability, resilience, and phase shifts in rocky subtidal
729 communities along the west coast of Vancouver Island, Canada. *Ecological*
730 *Monographs, 81*(2), 215-239. doi: 10.1890/10-0262.1

731 Weinberg, I., Bahlmann, E., Michaelis, W., & Seifert, R. (2013). Determination of fluxes and
732 isotopic composition of halocarbons from seagrass meadows using a dynamic flux
733 chamber. *Atmospheric Environment, 73*, 34-40. doi: 10.1016/j.atmosenv.2013.03.006

734 Wesely, M. L., & Hicks, B. B. (2000). A review of the current status of knowledge on dry
735 deposition. *Atmospheric Environment, 34*(12-14), 2261-2282. doi: 10.1016/S1352-
736 2310(99)00467-7

737 Wilson, T. W., Ladino, L. A., Alpert, P. A., Breckels, M. N., Brooks, I. M., Browse, J., . . .
738 Murray, B. J. (2015). A marine biogenic source of atmospheric ice-nucleating particles.
739 *Nature, 525*(7568), 234-238. doi: 10.1038/nature14986

740 Yakobi-Hancock, J. D., Ladino, L. A., Bertram, A. K., Huffman, J. A., Jones, K., Leaitch, W.
741 R., . . . Abbatt, J. P. D. (2014). CCN activity of size-selected aerosol at a Pacific coastal
742 location. *Atmospheric Chemistry and Physics, 14*(22), 12307-12317. doi: 10.5194/acp-
743 14-12307-2014

744 Yassaa, N., Peeken, I., Zöllner, E., Bluhm, K., Arnold, S., Spracklen, D., & Williams, J. (2008).
745 Evidence for marine production of monoterpenes. *Environmental Chemistry, 5*(6), 391-
746 401. doi: 10.1071/EN08047

747 Yokouchi, Y., Li, H. J., Machida, T., Aoki, S., & Akimoto, H. (1999). Isoprene in the marine
748 boundary layer (Southeast Asian Sea, eastern Indian Ocean, and Southern Ocean):
749 Comparison with dimethyl sulfide and bromoform. *Journal of Geophysical Research,*
750 *104*(D7), 8067-8076. doi: 10.1029/1998JD100013

751 Zeller, K. F., & Nikolov, N. T. (2000). Quantifying simultaneous fluxes of ozone, carbon
752 dioxide and water vapor above a subalpine forest ecosystem. *Environmental Pollution,*
753 *107*(1), 1-20. doi: 10.1016/S0269-7491(99)00156-6

754

755

Table 1. Summary of ODEs observed.

Date	**start time**	**end time**	**wind direction (°)**		**wind speed**	**ΔO_3**	**ΔO_x**	**ΔCO_2**	**ΔTerp.**
mo/day 2015	hr:min UTC	hr:min UTC	median local	Hysplit NAM12	m/s	ppbv	ppbv	ppmv	ppbv
07/16	09:14	14:00	WNW	WNW	1.1	-15.9	-	20.7	0.10
07/18	03:41	14:46	ESE	E	0.9	-16.0	-15.2	39.0	0.40
07/19	02:50	15:15	W initially, then E	W initially, then E	1.7	-23.3	-19.5	12.0	0.12
07/23	00:02	15:15	WNW	W	1.7	-19.5	-17.1	15.7	0.10
07/24	03:00	09:02	W	W	1.6	-18.1	-17.4	13.8	0.41
07/27	01:39	13:59	W initially, then E	W	1.7	-17.6	-15.6	15.5	0.32
07/28	01:59	14:01	WNW	WNW	2.1	-24.5	-23.8	14.3	0.07
07/30	02:23	10:03	W	W	2.5	-16.8	-16.0	51.7	0.64
07/31	07:04	10:09	WNW	WNW	2.2	-17.2	-16.8	32.4	0.19

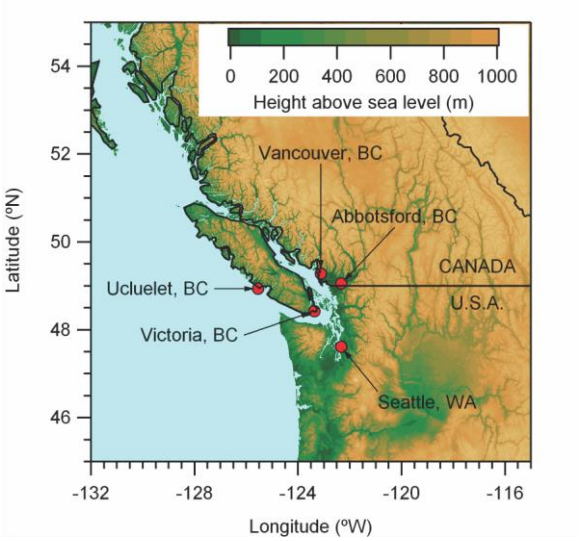

759

760 Figure 1. Map of the study region.

761

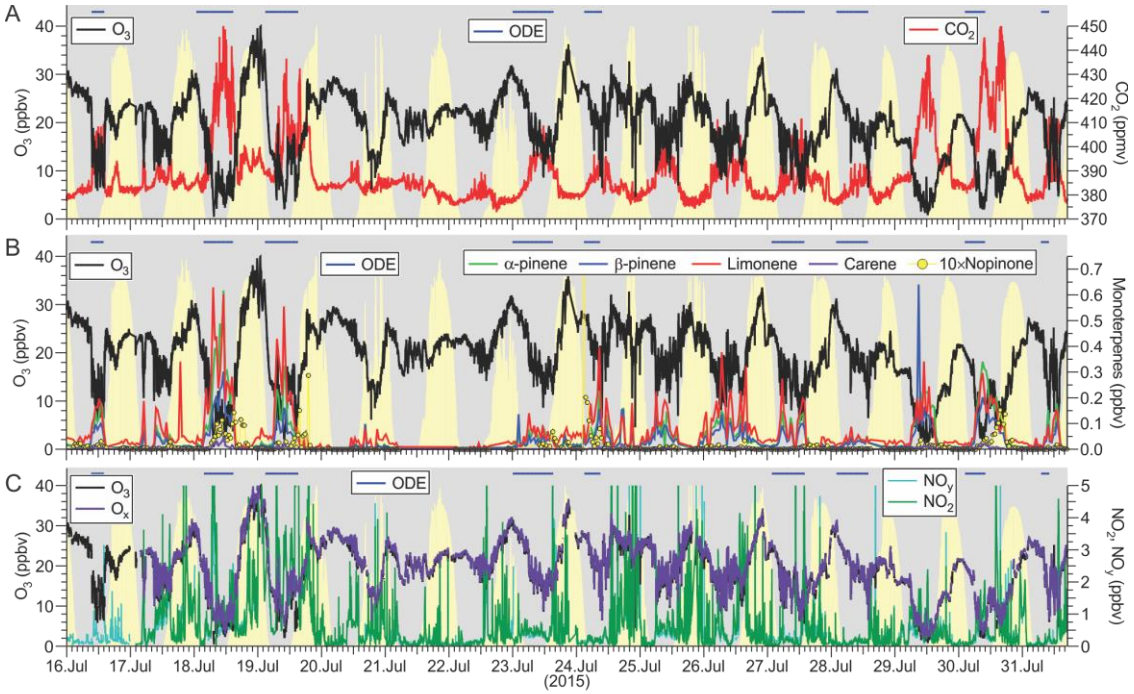

762

763 Figure 2. Time series of O_3 (left hand side, lhs) and CO_2 mixing ratios (A), monoterpene and
764 nopinone mixing ratios (B), and O_x (=O_3+NO_2), NO_2, NO_y mixing ratios (C). The blue lines
765 indicate O_3 depletion events identified using the criteria by McKendry et al. (2014). The
766 background colouring indicates the NO_2 photolysis frequency. The dates and times are in
767 coordinated universal time (UTC).

768

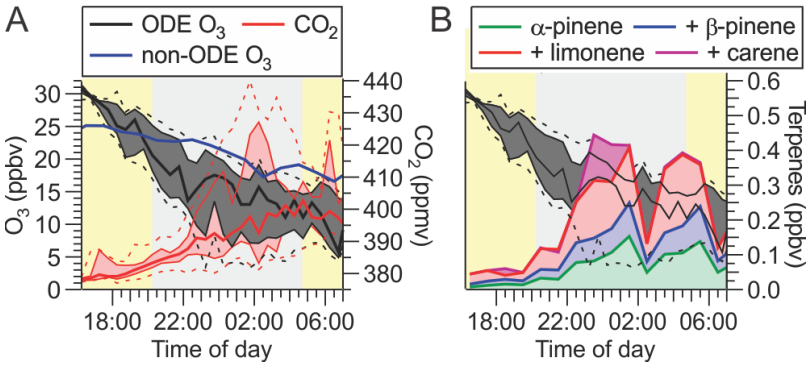

769

770 Figure 3. (A) O_3 (lhs) and CO_2 (rhs) mixing ratios as functions of (solar) time of day during
771 ODEs. The dashed lines indicate the 90th and 10th percentiles, whereas the shaded areas
772 encompass the 75th and 25th percentiles. The thick solid lines are the median values. Percentiles
773 were calculated over ½ hour bins. The median non-ODE O_3 time series is shown as a blue line.
774 (B) O_3 and terpene mixing ratios as functions of (solar) time of day during ODEs calculated
775 over 1 hour bins.
776

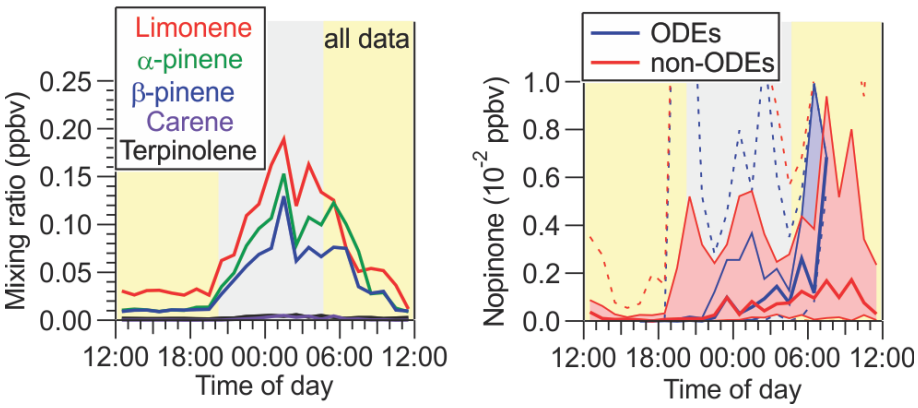

777

778 Figure 4. (A) Median mixing ratios of monoterpenes as functions of time of day. (B) Nocturnal
779 nopinone concentrations during ODE and non-ODE events as functions of time of day.

780

781

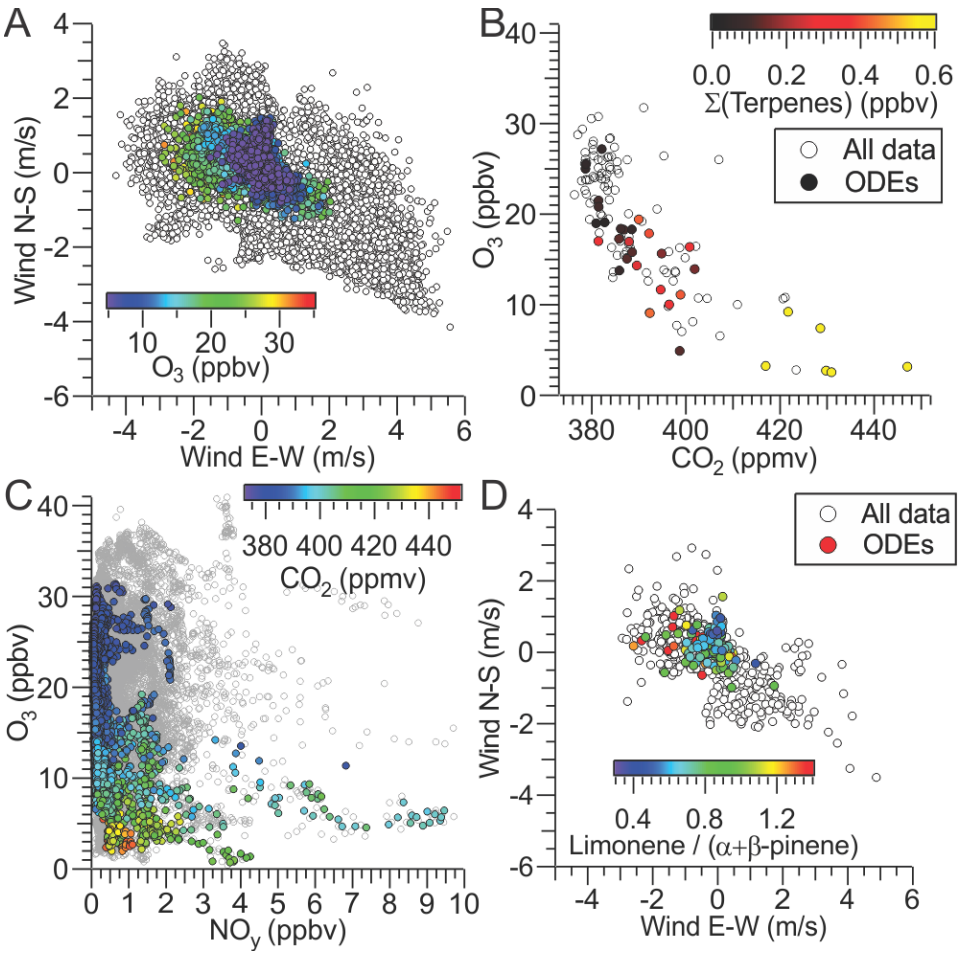

782

783 Figure 5. Correlations of O_3 mixing ratios with (A) wind direction and speed, (B) CO_2 mixing
784 ratios, colour-coded by the sum of α- and β-pinene and limonene mixing ratios, and (C) NO_2
785 mixing ratios, colour-coded by CO_2 mixing ratios. (D) Dependence of the limonene to (α- plus
786 β-pinene) ratio on wind direction and speed, plotted as their N-S and E-W components.
787

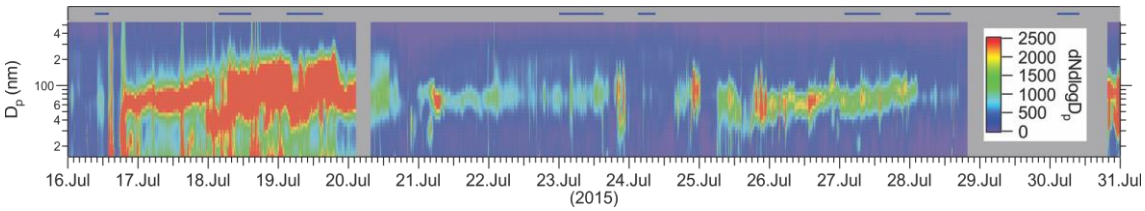

Figure 6. Time series of submicron aerosol size distributions.

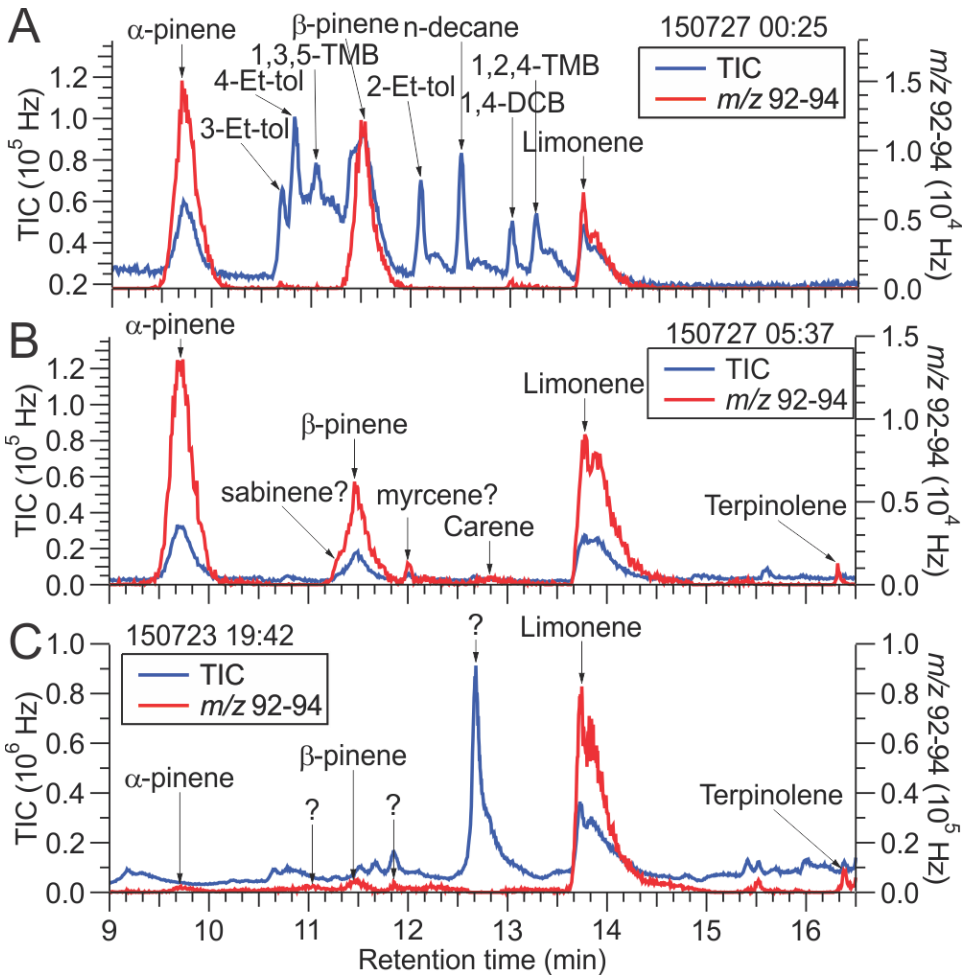

792

793 Figure 7. Total ion chromatogram (TIC, lhs) and selected (rhs) ion chromatograms of (A)
794 standard VOC calibration mixture, (B) ambient air during an ODE, and (C) headspace above
795 bull kelp (*nereocystis luetkeana*). Et-tol = ethyltoluene, TMB = trimethylbenzene, DCB =
796 dichlorobenzene.